

# Megahertz-frequency large-area optical modulators at 1.55 $\mu\text{m}$ based on solution-cast colloidal quantum dots

Sjoerd Hoogland, Vlad Sukhovatkin, Harnik Shukla, Jason Clifford, Larissa Levina, and Edward H. Sargent\*

Department of Electrical and Computer Engineering, University of Toronto, 10 King's College Rd., Toronto, Ontario M5S 3G4, Canada

\* Corresponding author: [ted.sargent@utoronto.ca](mailto:ted.sargent@utoronto.ca)

**Abstract:** We report the realization of large-area, communications-wavelength electro-optic modulators made via simple solution-casting onto an arbitrary substrate. The devices employ colloidal quantum dots synthesized in, and processed from, the solution phase. Devices exhibit greater than 30% modulation depth at the 1.55  $\mu\text{m}$  eye-safe wavelengths of interest in free-space optical communications. The devices retain considerable modulation depth beyond 1 MHz.

©2008 Optical Society of America

**OCIS codes:** (230.5590) Quantum-well, -wire and -dot devices; (130.4110) Modulators; (230.4110) Modulators; (250.4110) Modulators.

---

## References and links

1. D. Talapin and C. B. Murray, "PbSe nanocrystal solid-form-and-p-channel thin film field-effect transistors," *Science* **310**, 86–89 (2005).
2. N. Tessler, V. Medvedev, M. Kazes, S. Kan, and U. Banin, "Efficient near-infrared polymer nanocrystal light-emitting diodes," *Science* **295**, 1506–1508 (2002).
3. S. Hoogland, V. Sukhovatkin, I. Howard, S. Cauchi, L. Levina, and E. H. Sargent, "A solution-processed 1.53  $\mu\text{m}$  quantum dot laser with temperature-invariant emission wavelength," *Opt. Express* **14**, 3273–3281 (2006).
4. G. Konstantatos, I. Howard, A. Fischer, S. Hoogland, J. Clifford, E. Klem, L. Levina, and E. H. Sargent, "Ultrasensitive solution-cast quantum dot photodetectors," *Nature* **442**, 180–183 (2006).
5. K. W. Johnston, A. G. Pattantyus-Abraham, J. P. Clifford, S. H. Myrskog, D. D. MacNeil, L. Levina, and E. H. Sargent, "Schottky-quantum dot photovoltaics for efficient infrared power conversion," *Appl. Phys. Lett.* **92**, 151115 (2008).
6. J. M. Kahn and J. R. Barry, "Wireless infrared communications," *Proc. IEEE* **85**, 265–298 (1997).
7. A. V. Jelalian, *Laser Radar Systems* (Artech House, 1991).
8. H. Rossmann, A. Schulzgen, F. Hennenberger, and M. Muller, "Quantum Confined DC Stark Effect in Microcrystallites," *Phys. Status Solidi* **159**, 287–290 (1990).
9. U. Woggon, S. V. Bogdanov, O. Wind, K.-H. Schlaad, H. Pier, C. Klingshirn, P. Chatziagorastou, and H. P. Fritz, "Electro-optic properties of CdS embedded in a polymer," *Phys. Rev. B* **48**, 11979–11986 (1993).
10. S. A. Empedocles and M. G. Bawendi, "Quantum-confined Stark effect in single CdSe nanocrystallite quantum dots," *Science* **278**, 2114–2117 (1997).
11. V. L. Colvin, K. L. Cunningham, and A. P. Alivisatos, "Electric field modulation studies of optical absorption in CdSe nanocrystals: Dipolar character of the excited state," *J. Chem. Phys.* **101**, 7122–7138 (1994).
12. E. J. Klem, L. Levina, and E. H. Sargent, "PbS quantum dot electroabsorption modulation across the extended communications band 1200–1700 nm," *Appl. Phys. Lett.* **87**, 053101 (2005).
13. D. Yu, C. Wang, and P. Guyot-Sionnest, "n-Type conducting CdSe nanocrystal solids," *Science* **300**, 1277–1280 (2003).
14. P. Guyot-Sionnest and C. Wang, "Fast voltammetric and electrochromic response of semiconductor nanocrystal thin films," *J. Phys. Chem. B* **107**, 7355–7359 (2003).
15. W. K. Woo, K. T. Shimizu, M. V. Jarosz, R. G. Neuhauser, C. A. Leatherdale, M. A. Rubner, and M. G. Bawendi, "Reversible charging of CdSe nanocrystals in a simple solid-state device," *Adv. Mater.* **14**, 1068–1071 (2002).

## 1. Introduction

Solution-processed materials have recently shown promising performance in applications as diverse as transistors [1], light emission [2] and lasing [3], optical detection [4], and photovoltaics [5]. These high-performance colloidal quantum dot devices did not in general exhibit the capacity to respond in time faster than 1 millisecond; however, for colloidal quantum dots to extend their impact into communications and information processing, greatly increased speeds will be required.

Large-area, high-speed devices are of particular interest in free-space optical communications [6]. The high cost of epitaxial quantum well devices stands in the way of economical line-of-sight systems of this type.

Here we report devices based on quantum size-effect-tunable colloidal quantum dots that achieve modulation at the 1.55  $\mu\text{m}$  wavelength at which powerful, stable optical sources are widely available; at which the eye is nonabsorbing and thus eye-safety is assured to 1 J/cm<sup>2</sup>; and wherein light is transmitted through the atmosphere over > 2 km distances even under cloudy conditions [7]. The devices exhibit 30% modulation depth, a 120 kHz 3-dB bandwidth, and significant response to 1 MHz.

## 2. The quantum-confined Stark effect in ensembles of colloidal quantum dots possessing randomly-oriented built-in dipoles

The reduced-dimensionality materials system employed herein exhibits the quantum-confined Stark effect. We summarize briefly this phenomenon, particularly as it applies to ensembles of colloidal quantum dots that possess randomly-oriented built-in dipoles.

The quantum-confined Stark effect describes the change in the spectrum of the real and imaginary parts of refractive index under the application of an electric field in a quantum-confined structure such as a quantum well, wire, or dot. Here we focus specifically on the change in the absorption spectrum. In contrast with bulk semiconductors, in which the main influence of an electric field is ionization of electron-hole pairs [8], the quantum-confined Stark effect produces a redshift in the excitonic absorption when the electric field is applied along a quantum-confined direction [9]. Two factors favor a strong absorption modulation response in quantum-confined systems: a large exciton binding energy, and an increased oscillator strength, compared to unconfined systems. The redshift arises because the shape of the (originally-symmetric) confining potential is distorted by the field such as to lower the energy associated with transitions between the quantum-confined valence and conduction band states. It should be noted that higher-lying states' transition matrix elements are also influenced by the applied field, redistributing oscillator strength among absorption features at energies well above the quantum-confined bandgap.

If, however, a built-in dipole exists within a quantum dot, the spectral shift will depend on the alignment of the applied field and the built-in dipole [10, 11, 12]. The application of an external field additive with that due to the dipole will result in a redshift. If the external and dipolar fields are antiparallel, a blueshift will result since the external field acts to reduce the net field inside the well.

The Stark effect acting on materials having built-in dipoles has been extensively reported in colloidal quantum dots. The built-in dipole is attributed to electrons trapped on the nanoparticle surface [10, 11]. Since electrons are, at room temperature, continually undergoing trapping and detrapping, the orientation and amplitude of the built-in dipole in each dot diffuses over time. In a colloidal quantum dot solid consisting of many nanoparticles, the dipole orientation and amplitude are also randomly distributed in space over the ensemble.

As a result, for an individual dot, whether a red or blue shift will occur will vary randomly based on the ever-changing alignment between the built-in dipole and the applied field. For a large ensemble of dots having randomly-oriented built-in dipoles – typically half of which may have a component aligned with the applied field, the other half antiparallel – the effect will be that approximately half of the dots redshift, and half blueshift. The result is a loss in absorbance near the ensemble material's excitonic peak, and a slight increase in absorbance in

the wings. If the polarity of the applied field sign is reversed, the parallel and antiparallel-aligned dots switch roles, and the modulation in the absorption spectrum remains a broadening.

The amplitude of the maximum change in absorption has previously been shown to change in proportion with the square of the applied field [8].

In quantum-confined systems, the choice of the spatial dimensions of the confining system offer quantum-size-effect tuning of the absorption features, and thus enable selection the spectral position of the strongest absorption-modulation features. The present work concerns PbS colloidal quantum dots, a system chosen because it allows us access to the 1.5  $\mu\text{m}$  wavelength band of interest in free-space optical communications.

### **3. Past reports of colloidal quantum dot optical modulator application-relevant performance**

Beyond fundamental spectroscopy, it is of interest to exploit colloidal quantum dots' electro-absorption behavior in devices. Particularly attractive is colloidal quantum dots' compatibility with large-area, low-cost optoelectronics. Simple solution-coating of these materials from a solvent onto an arbitrary substrate, with no requirement for lattice-matching, makes colloidal quantum films simple to deploy.

Nanocrystals embedded in an insulating polymer matrix [11] or sandwiched between two insulating electrodes [12] have been used to demonstrate an electric-field-induced change in the excitonic absorbance due to ground or excited state dipoles. While absorption changes  $\Delta\alpha/\alpha_0$  of  $10^{-5}$  were sufficient to elucidate spectroscopically the properties of these materials, they were far from providing useful contrast in an optical modulator. Usefully large changes in absorbance have been realized in colloidal quantum dots via electrochemical modulation [13]; however, these cells were reported to have very slow switching times. In one report, 40% absorption bleaching was observed but took seconds [14] while, in another report, 25% photoluminescence quenching was observed at 20 Hz [15].

In sum, capacitive devices were potentially fast, but showed extremely weak modulation since the field across the nanocrystals was small (falling instead across blocking contacts or insulating matrix); and devices based on current flow showed deep modulation, but Hz or slower frequencies.

### **4. Our approach: Device fabrication and materials properties**

The Stark effect can in principle be exploited without compromise: it can be both deep in amplitude and rapid in response, for the field used to accomplish Stark effect modulation is communicated at the speed of electromagnetic waves. It is the practical limitations of real solid-state materials that account for the failure, to date, to produce a promising Stark effect colloidal quantum dot device. These limitations – arising from the widespread practice of passivating surface states using insulating ligands – are not fundamental.

We therefore sought to show that the ostensible compromise between speed and depth of modulation can be overcome through materials engineering. To produce, within a practical solid-state device, a Stark effect modulation with substantial megahertz-frequency response, we sought to passivate long-lived trap states attributable to unpassivated sites on the nanoparticles' surfaces; but to do so using a conductive organic ligand, benzenedithiol, in order to minimize the medium's dielectric relaxation time and thus drive speed of response into the MHz regime.

We synthesized lead sulfide nanocrystals via the organometallic route. The resultant oleate-capped nanoparticles were precipitated and then redispersed in toluene. Within a dry nitrogen environment, we exchanged the capping ligands to the shorter butylamine and redispersed the exchanged nanoparticles into chloroform. We spincoated the nanocrystals atop a commercially-available ITO-covered glass substrate to a thickness of 230 nm (resulting in optical density of 0.2 at 1.55  $\mu\text{m}$ ) and immediately immersed them in a freshly-prepared 1 mM solution of 1,4-benzenedithiol in anhydrous acetonitrile. We left the sample for 30

minutes, after which we rinsed with toluene and immediately transferred to the vacuum chamber for sputtering. We sputtered gold electrodes with a diameter of 300  $\mu\text{m}$  to a thickness of 100 nm. The device is shown schematically in Fig. 1.

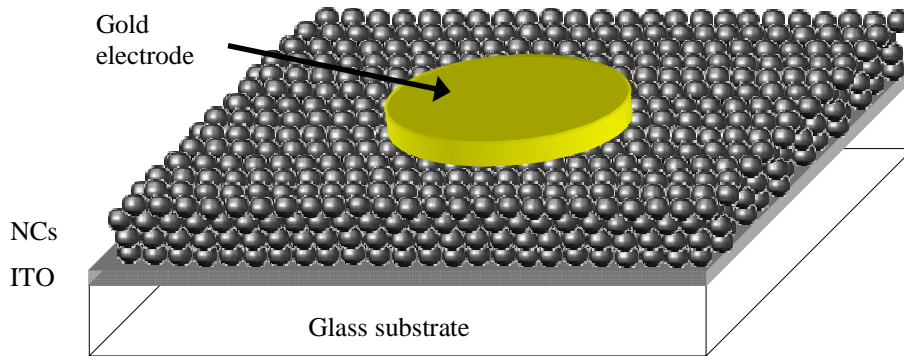


Fig. 1. Colloidal quantum dot electro-absorption modulator architecture. In the experiments presented herein, light is incident from the bottom. It passes through the transparent glass substrate, through the colloidal quantum dot film, reflects off of the gold electrode, and is passed again through the film and substrate. Measurements reported herein are thus made in reflection mode.

We show in Fig. 2 both side and top views of a benzenedithiol-treated nanocrystal film on silicon. The nanoscale cracks do not penetrate down to the substrate, as attested to by the lack of short circuits observed in the devices' I-V characteristics.

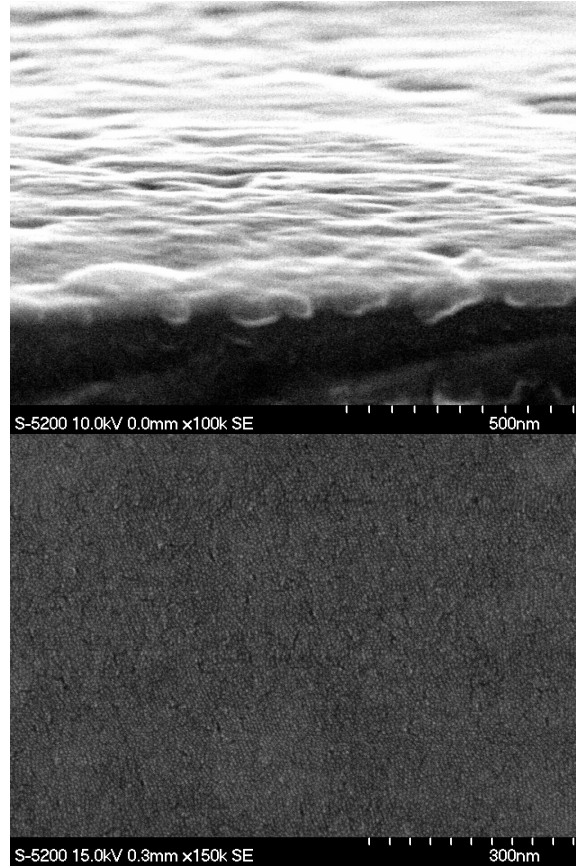


Fig. 2. Electron micrographs of a ~50 nm thick layer of benzendithiol-treated nanocrystal film on silicon. The top image shows a cross-sectional view; the lower image shows a top-surface view. Close-packing of the nanocrystals may be observed; nanoscale cracks do not penetrate to the substrate.

## 5. Device performance

We present in Fig. 3 the spectral changes in absorption ( $\Delta\alpha/\alpha_0 = (\alpha(V=0V) - \alpha(V))/\alpha(V=0V)$ ) for different applied DC biases and polarities.

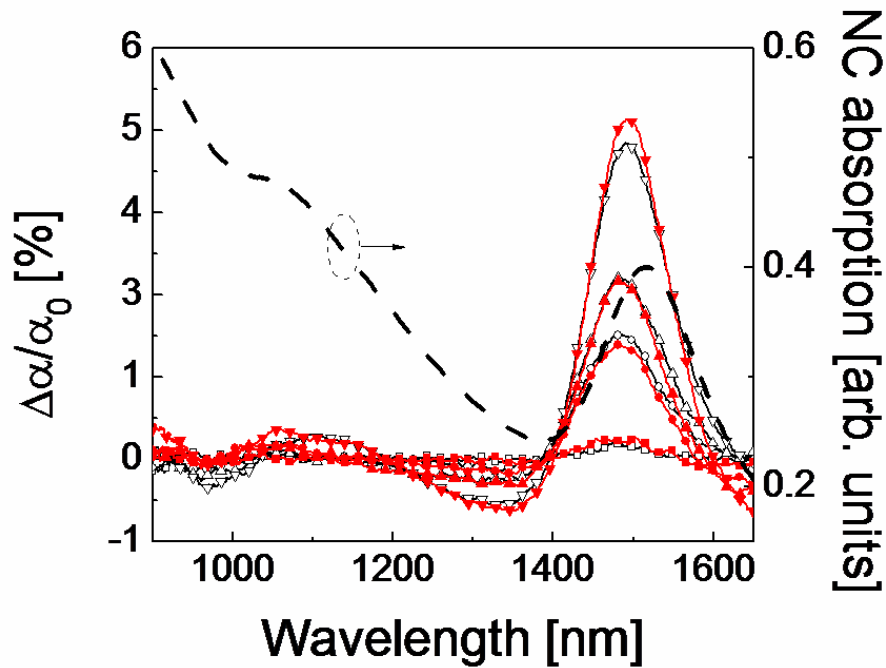


Fig. 3. Change in absorption under both positive and negative DC biases as a function of wavelength. Red corresponds to positive bias while black corresponds to negative bias. The increasing-amplitude spectra are for +/-1 V, +/-3 V, +/-4 V, and +/-6 V.

For both positive and negative bias, the shape and amplitude of the absorption modulation features are substantially the same. At and near the excitonic peak, the applied field reduces the absorption. In the wings, the absorption is slightly increased. In sum, the application of the field results in a broadening of the absorption spectrum.

The spectral features of these devices, as well as their invariance with applied field polarity, are consistent with the mechanism presented in Section 2: in an ensemble of quantum dots possessing built-in dipoles, those having dipoles parallel with the applied field experience a redshift; those antiparallel a blueshift; and the effect appears in the macroscopic device as an ostensible broadening, most strongly of the first excitonic feature – the most highly-polarizable of the quantum dots' transitions.

As previously observed [11, 12], the depth of modulation is strongest near the first excitonic transition.

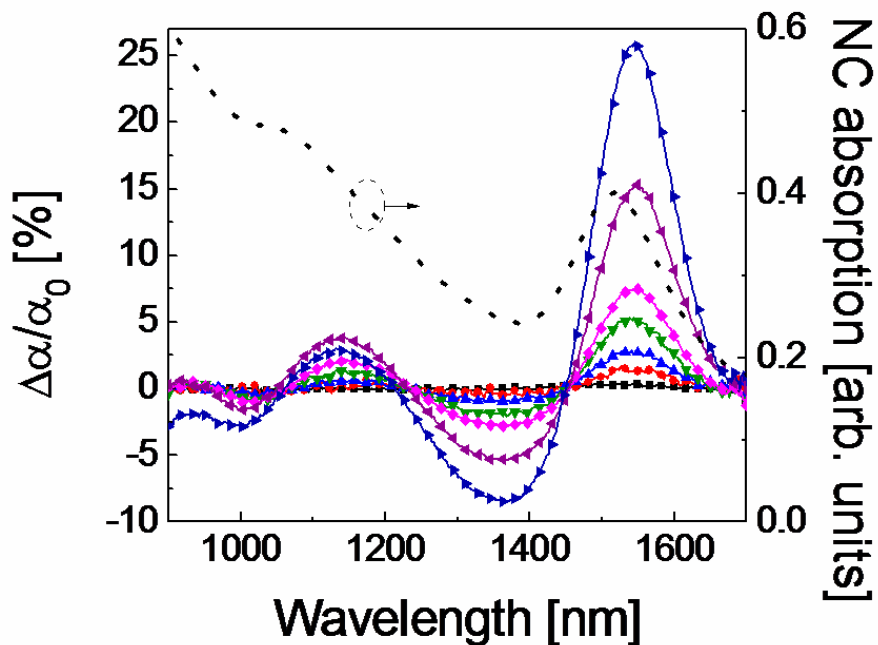


Fig. 4. Change in absorption under large negative DC biases as a function of wavelength. Curves with increasing amplitude of absorption change correspond to -1 V, -3 V, -5 V, -7 V, -9 V, -11 V, and -12 V bias. The maximum absorption change exceeded 25% for an applied DC voltage of -12 V. Note that the vertical scale bar spans 35% compared to the 7% span of Fig. 3.

We present in Fig. 4 one of the large DC changes in absorbance that we observed. The peak change is 25%. We attribute the large changes in absorbance compared to previous works to our use of conductive linker molecules which ensured that a significant portion of the applied bias fell across the nanoparticles themselves, instead of across substantially insulating ligands.

We now turn to the temporal response of these devices. We employed a 10 or 40  $\mu\text{s}$  voltage pulse with variable amplitude at a repetition rate of 500 Hz. We probed the absorption change using a continuous-wave diode laser tuned to the wavelength at which the maximum change in absorption occurred in the DC case. The reflected signal was coupled to a fast photodiode.

We present in Fig. 5 the response to modulation for negative voltage pulses, and in Fig. 5(b) for positive voltage pulses.

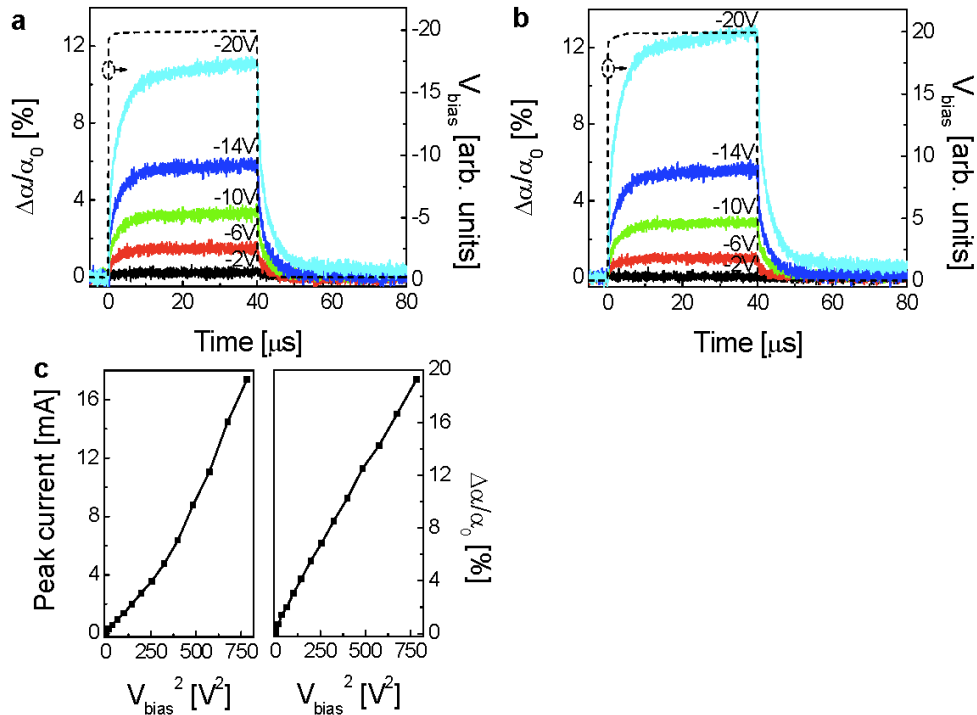


Fig. 5. Temporal dependence of the change in absorption at the wavelength of maximum modulation. In (a) and (b) we report the absorption change in response to the application of a periodic train of 40  $\mu\text{s}$  voltage pulses. In (a) we report for negative pulses while in (b) for positive. Pulse amplitudes of 2, 6, 10, 14, and 20 V were applied. The measured fall and rise characteristics fit well to a single exponential with characteristic time 4  $\mu\text{s}$ . The amplitude and temporal response of absorption change are substantially invariant with field polarity. In (c) we report the peak current and peak absorption change amplitude as a function of the square of the bias voltage.

Both bias polarities give rise to an absorption decrease at the probe wavelength with amplitudes exceeding 10% of the unbiased absorption. The rising edges and falling edges of the modulation response are described by single-exponential functions with characteristic times of 4  $\mu\text{s}$ . The fact that the amplitude of the change in absorption does not follow the two-slope behaviour of the current vs. voltage-squared dependence, but instead is consistently linear with the squared peak applied field, reinforces the attribution of the observed absorption modulation to field rather than carrier injection due to current.

The speed of absorption recovery determines the modulation bandwidth of the device. We investigated the dependence of the absorption modulation amplitude on the frequency of electric field modulation. To investigate from DC to 100 kHz, we applied a sinusoidal AC (10 V peak-to-peak) modulation atop a 5 V DC bias and used a lockin amplifier to detect the change in absorption at the applied frequency. As seen in Fig. 6(a), the frequency response was substantially flat out to about 100 kHz. To assess the frequency response beyond 100 kHz, we applied a double-pulsed temporal voltage profile that mimicked a single oscillation having modulation frequency  $1/2\Delta t$  and monitored the response using a digitizing oscilloscope. Figure 6(a) shows that the frequency rolloff agrees well between lockin and double-pulse measurements over the significant range of overlapping frequencies. The modulation response reveals rolloff to 3 dB down by 120 kHz. Substantial modulation depth – greater than 4% – is retained even out to 1 MHz.



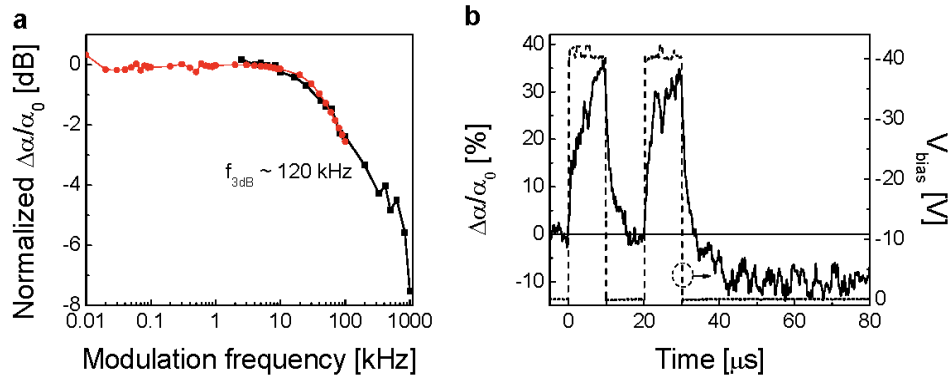


Fig. 6. Modulation electrical frequency spectrum and 50 kHz pulse modulation response. a, Modulation bandwidth as measured at the peak Stark-wavelength of the 230 nm thick device, obtained by applying a single oscillation of the set frequency with an amplitude of -30 V (black) or a frequency-variable sinusoidal bias (red). The frequency response exhibits a 3 dB bandwidth of 120 kHz. b, Absorption change (solid line) in response to the application of a voltage double-pulse (dashed line). The maximum change in absorption is more than 30% ( $\lambda_{\text{probe}}=1500$  nm) at an effective frequency of 50 kHz.

To obtain the largest change in absorption that could be achieved under a modulated bias we applied a single burst of double voltage pulses to the sample. The two pulses had a duration of 10  $\mu\text{s}$  and were separated by 10  $\mu\text{s}$ , thus achieving an effective 50 kHz modulation frequency. This frequency is well within the modulation bandwidth of the device. The maximum obtainable change in absorption was 33% for a voltage amplitude of 40 V (Fig. 6(b)) at a probe wavelength of 1500 nm. The absorption recovers entirely between the voltage pulses, while a long-lived induced absorption change remains after the second voltage pulse. We attribute this to heating.

The approach employed herein is compatible with large-area low-cost devices. Processing in cleanroom conditions would aid in further expanding device diameter while keeping acceptable yield.

## 6. Summary

We have demonstrated a simple method to create efficient Stark effect modulation device which can be readily fabricated from solution. These devices exhibited more than 30% peak absorption modulation at the 1.55  $\mu\text{m}$  eye-safe wavelengths with modulation bandwidths of 120 kHz and considerable modulation depth at 1 MHz.